This article has been accepted for publication in a future issue of this journal, but has not been fully edited. Content may change prior to final publication. Citation information: DOI 10.1109/TPWRD.2015.2420657, IEEE Transactions on Power Delivery

Active Voltage Feedback Control for Hybrid Multi-terminal HVDC System Adopting Improved Synchronverters

Shuan Dong, Yong-Ning Chi, Yan Li

***Abstract*—In this paper, we propose an idea to integrate more renewable energy into the existing China power grid and to provide remote islands with reliable power supply. The idea is to expand the existing point-to-point LCC HVDC transmission link into a hybrid multi-terminal HVDC (hybrid MTDC) system, which contains both LCC stations and VSC stations. Accordingly, this paper proposes a novel control strategy for this system named active voltage feedback control, which features that it does not need any high speed communication system under various disturbances, such as wind speed variations, load fluctuations, faults, etc. The paper also adds secondary frequency regulation to synchronverter, which is one way of combining VSC converter with synchronous machine behavior. Then the paper applies an approach to limit its current under fault conditions. Finally the whole hybrid MTDC system is modeled in PSCAD/EMTDC. Simulation results show that the improved synchronverter is able to achieve secondary frequency control, and the presented *active voltage feedback control* works very well when exposed to various disturbances.**

***Index Terms*—Active voltage feedback control, hybrid MTDC, DC grid, synchronverter, secondary frequency control, virtual SG.**

I. Introduction

In China, 67.8% of available hydropower resources are located in the southwest area, and 40.0% of coal resources are located in the far western region of Xinjiang. But load centers are mainly distributed in the central part and eastern coastal areas. Due to this inverse distribution between resources and loads, many point-to-point LCC HVDC lines have been built in the name of " Western Power to East " to meet the intense power demand of the eastern area and to boost the economy of the western part at the same time.

As normal fossil energies will be finally used up, it is very likely to turn to renewable energies in future. But wind and solar energy have intrinsic intermittence and fluctuation, so their integration will inevitably pose serious challenges to the power grid's stability. E.g., even though some remote islands are near some offshore wind farms, they cannot get reliable power supply from these wind farms directly.

If the existing LCC HVDC connection in China could be expanded into a hybrid MTDC system [1] which integrates renewable resources and supplies the remote islands, this system will not be limited by transmission distance, and can: (i) offset the randomness from different areas; (ii) smooth the power fluctuation by more dc capacitors and inertia [2]; (iii) share frequency control reserve within the dc grid [3]; (iv) combine advantages of LCC HVDC and VSC HVDC, because the former is more economic, whereas the latter can supply a weak grid, control active power and reactive power independently, etc. [4]- [6]

In terms of VSC control, conventional methods can ensure that VSC's current injection into the grid is clean sinusoidal, e.g., voltage-oriented vector control [7] or virtual-flux-based direct power control (VF-DPC) [8]. But they all rely on phase lock loop (PLL), which may deteriorate VSC's performance in transients especially in a weak grid [9][10], let alone regulate its grid frequency. Besides, in weak grids where the connecting impedance between converter and grid is high, the load angle is larger, and the voltage is more sensitive to reactive power fluctuation. So angle and voltage stability problems are more prominent. Synchronverter [11] can run normally under weak grid conditions, because it: (i) does not need PLL during normal operation; (ii) introduces a virtual rotor to emulate the dynamic behaviors of synchronous machine(SM), and contributes inertia and damping to the grid. So it greatly improves the grid's angle stability; (iii) is better than a real SM in some aspects, as some parameters can be designed freely regardless of SM's physical limits; (iv) can regulate the voltage at the point of common coupling (PCC), and improve the grid's voltage stability; (iv) can regulate the grid frequency. Moreover, by introducing synchronverter, many excellent research results, theories and methods in conventional power system might be transplanted to our current power grid, where the share of converter-interfaced generation units keeps increasing. However, the synchronverter in [11]: (i) cannot realize secondary frequency regulation when necessary, which means that there probably exists a permanent frequency offset in the grid even after frequency regulation. (ii) cannot avoid overcurrent situations. In this paper, the improved synchronverter will be able to realize secondary frequency control, and limit its current in faults conditions.

For controls of hybrid MTDC system, master-slave control

Manuscript received September 1; 2014, revised November 26, 2014, February 1, 2015, and April 2, 2015. This work was supported in part by National High-Tech R&D Program of China (2013AA050601).

S. Dong, Y.-N. Chi and Y. Li are with the Renewable Energy Department, China Electric Power Research Institute (CEPRI), Beijing 100192 China (e-mail: profshuan@gmail.com; chiyn@epri.sgcc.com.cn; liyan@epri.sgcc.com.cn)

This article has been accepted for publication in a future issue of this journal, but has not been fully edited. Content may change prior to final publication. Citation information: DOI 10.1109/TPWRD.2015.2420657, IEEE Transactions on Power Delivery

[13] needs a high speed communication system during normal operation, so it is less reliable. Literature [14] uses a control which resembles voltage margin control used in VSC MTDC system [15] and can effectively reduce its reliance on high speed communication systems, but it cannot regulate the grid frequency. The control strategies given by literature [16][17] are also not aiming to integrate renewable energy, share frequency control reserve in dc grid, and terminate its reliance on high speed communication system at the same time, so they cannot be used here, too.

In this paper, we: (i) propose an idea to integrate large capacity renewable energy into the existing China power grid, provide remote islands with reliable power supply, and regulate their frequencies. Our idea is to expand an existing traditional point-to-point LCC HVDC line into a hybrid MTDC system; (ii) improve the synchronverter; (iii) propose a novel steady state control strategy named *active voltage feedback control* for this system. This control strategy features that: (i) does not rely on telecommunication systems; (ii) can realize large scale renewable energy integration; (iii) ensures that the frequency control reserve can be shared through the whole dc grid.

This paper is structured as followed: Part II mainly describes the topology of the dc system after expansion, part III introduces the improved synchronverter, and part IV proposes the *active voltage feedback control*. In part V the whole hybrid MTDC system is modelled in PSCAD/EMTDC. Thereafter a comparison is done between the original synchronverter and the improved one. Then the proposed *active voltage feedback control* is tested and analyzed under disturbances, including various faults. At last, conclusions are drawn in part VI.

II. Description Of Hybrid MTDC System's Topology

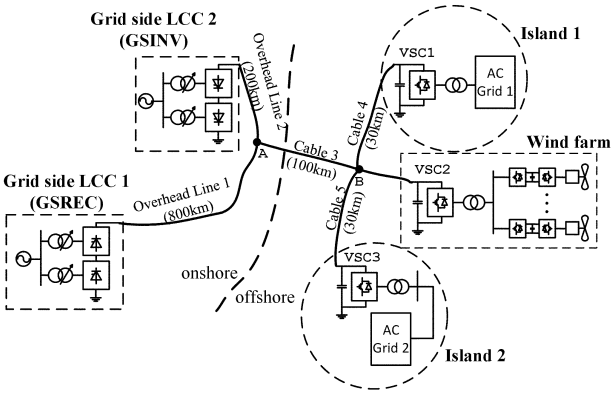

Fig. 1. Single line diagram of the hybrid MTDC system

As shown in Fig. 1, there is a traditional point-to-point LCC HVDC line on land rated 1000MW and 500kV. The rectifier station (GSREC) is located in the western energy-rich area, and connected to a strong grid (SCR=8) with sufficient active and reactive power reserves. The inverter station (GSINV) is built in the eastern coastal part, and SCR of its connected ac grid is about 5.5. After expansion, GSINV will remain unchanged, and GSREC's rated power output will increase to 1500MW.

There are abundant wind energy resources in the sea 110km eastward from point A, so a wind farm rated 430MW is planned there, and the wind power is sent out through a VSC station called VSC2. On one hand, wind speed at sea is not influenced by surface roughness, so the wind shear is relatively small, on the other hand, visual pollution, noise pollution and even the impact on birds can be avoided or reduced, because the offshore wind farm is far away from the land.

There are two islands near the offshore wind farm, Island 1 to the north and Island 2 to the south. As Fig. 2(a) shows, there have been two power plants which rate 165MW and 85MW respectively on Island 1. To ensure reliability of its power supply, the ac grid on this island (AC Grid 1) is a ring structure with rated voltage of 110kV. Now a VSC station (VSC1) rated 200MW is planned on Island 1, then Plant 1 will be shut down. In the south, the ac grid rated voltage on Island 2 (AC Grid 2) is also 110kV, as Fig. 2(b) shows. A VSC station rated 250MW and a PV station rated 50MW will be built on Island 2 to guarantee the power supply. Note that real rotary inertia exists in AC Grid 1, whereas does not exist in AC Grid 2.

The selection of dc line routes is beyond our scope, and they are simply chosen as Fig. 1 shows.

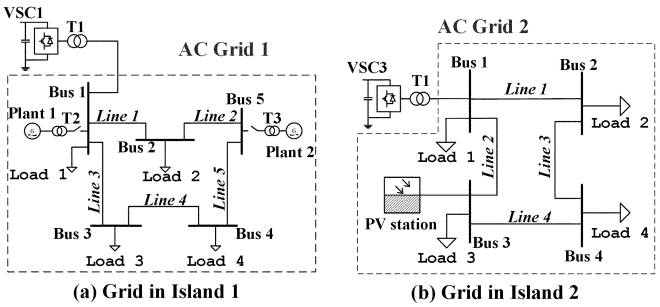

Fig. 2. Network topologies of AC Grid 1 and AC Grid 2

III. The Improved Synchronverter

Though when synchronverter is defined, it only refers to inverters that mimic synchronous generators [11]. In fact, it can also mimic a synchronous motor by simply changing the sign of active power reference value. Here we interpret its definition as VSC converters that mimic SMs.

In this part, on the one hand, we propose adding a switchable integral frequency feedback loop to synchronverter. In this way, secondary frequency control can be achieved in isolated control areas. Note that traditionally, "primary frequency control" is local, automatic control action that adjusts the active power output of the generating units in direct response to the measured shaft rotational speed variations. "Secondary frequency control" is a wide area control that usually relies on a proportional integral (PI) controller, filters, or heuristics to restore the frequency and the interchanges with other systems to their target values [18]- [21]. Further talk is needed on differences between frequency controls exercised by converter-interfaced and traditional generator units. In this paper, we simply think that primary control will results in a permanent frequency offset, and secondary control can restore the frequency with no error.

On the other hand, as synchronverter in [11] cannot limit its current output under fault conditions. We also add a switchable current limit loop to synchronverter to avoid overcurrent.

This part is organized as follows: First, a virtual SM model

This article has been accepted for publication in a future issue of this journal, but has not been fully edited. Content may change prior to final publication. Citation information: DOI 10.1109/TPWRD.2015.2420657, IEEE Transactions on Power Delivery

will be given. Then as its counterpart, the improved synchronverter model will be introduced. Note that their corresponding variables will be represented by same symbols.

A. Virtual synchronous machine

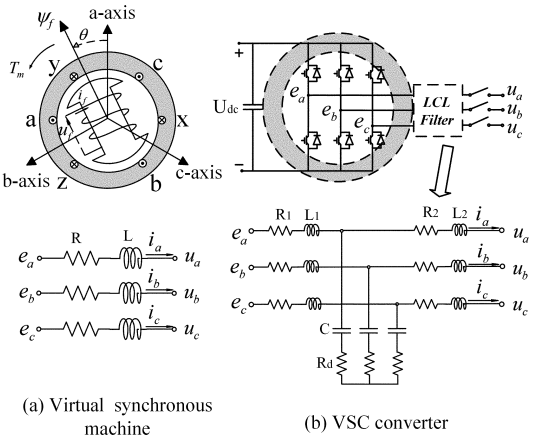

(a) Virtual synchronous machine (b) VSC converter

Fig. 3. Virtual synchronous machine and VSC converter

In synchronverter's case, it is our main concern to make converters have the same synchronization mechanism like SM. I.e., its virtual rotor will swing like a real rotor when feeling imbalanced torque. So our virtual SM is simplified like this: (i) the stator and rotor are symmetrical and their surfaces are sufficiently smooth; (ii) does not take flux saturation into consideration; (iii) MMF in the air gap is sine shaped; (iv) there is no damping winding; (v) mutual inductance between stator windings is 0; (vi) its synchronous reactance is smaller than that in real SM. (vii) number of pole-pairs is considered to be 1; (vii) stator windings are star connected without neutral line.

The positive directions of voltages, currents and flux axis can be found in Fig. 3, the positive directions of flux and corresponding current meet the right hand rule, so we get:

$$\begin{cases} \psi_S = L_{SS} i_S + M_f i_f \overline{\cos\theta} \\ e = R i_S + L\dfrac{di_S}{dt} + u \end{cases} \tag{1}$$

Where the stator flux $\psi_s = [\psi_a\ \psi_b\ \psi_c]^T$, the stator current $i_s = [i_a\ i_b\ i_c]^T$, the inner voltage $e = [e_a\ e_b\ e_c]^T$, the terminal voltage $u = [u_a\ u_b\ u_c]^T$, the stator windings' self-inductance is L, the stator resistance is R, the inductance coefficient matrix $L_{SS} = LE_{3\times3}$, M_f is the excitation inductance, i_f is the excitation current, θ is the rotor angle, and

$$\overline{\cos\theta} = \left[\cos\theta \quad \cos(\theta - \frac{2\pi}{3}) \quad \cos(\theta + \frac{2\pi}{3})\right]^T \tag{2}$$

Without considering the induced electromotive force produced by rotor excitation current, the inner voltage e is:

$$e = -\frac{d\psi_S}{dt} = \omega M_f i_f \overline{\sin\theta} \tag{3}$$

Where $\omega = \dfrac{d\theta}{dt}$,

$$\overline{\sin\theta} = \left[\sin\theta \quad \sin(\theta - \frac{2\pi}{3}) \quad \sin(\theta + \frac{2\pi}{3})\right]^T \tag{4}$$

The magnetic field energy stored in the machine is:

$$W_m = \frac{1}{2}\begin{bmatrix} i_S{}^T & i_f \end{bmatrix}\begin{bmatrix} L_{SS} & L_{RS} \\ L_{RS}^T & M_f \end{bmatrix}\begin{bmatrix} i_S \\ i_f \end{bmatrix} \tag{5}$$

Where $L_{RS} = M_f \overline{\cos\theta}$.

Supposing positive direction of the electromagnetic torque T_e and that of the rotor speed ω are opposite, we get [22]:

$$T_e = -\frac{\partial W_m}{\partial \theta} \tag{6}$$

According to (5) (6), the electromagnetic torque T_e is:

$$T_e = M_f i_f i_S{}^T \overline{\sin\theta} \tag{7}$$

The reactive power output of the machine is expressed by:

$$Q = -\omega M_f i_f i_S{}^T \overline{\cos\theta} \tag{8}$$

Without considering the friction, the mechanical dynamics is:

$$J\frac{d\omega}{dt} = T_m - T_e - D_f(\omega - \omega^*) \tag{9}$$

Where J is rotary inertia, T_m is the input torque, D_f is the power drooping coefficient, and ω^* is the reference value of angular velocity. Note that for real machines, the friction torque should always oppose rotor's motion, so D_f is not friction coefficient here. Besides, further research is needed on how to include damper windings in the synchronverter, and whether that could significantly improve synchronverter's performance as well as benefit the grid. This paper will not discuss it further.

B. The improved synchronverter

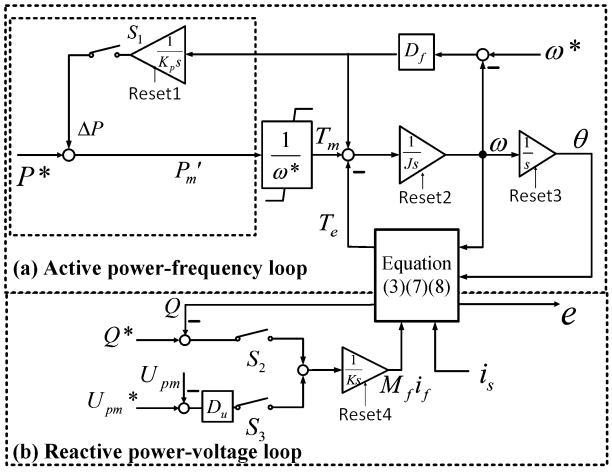

Fig. 4. Control diagram of the improved synchronverter

First, the equivalency between VSC converter and virtual machine is only for fundamental components, without considering higher harmonics. Hence in Fig. 3, it is reasonable to make the following approximation [23]:

$$\begin{cases} R = R_1 + R_2 \\ L = L_1 + L_2 \end{cases} \tag{10}$$

When controlling the VSC converter, it is considered as a virtual SM. Its rotating virtual rotor only has a field winding. Its rotatory inertia, rotating speed and rotor angle are respectively J, ω and θ. The VSC converter's ac output

This article has been accepted for publication in a future issue of this journal, but has not been fully edited. Content may change prior to final publication. Citation information: DOI 10.1109/TPWRD.2015.2420657, IEEE Transactions on Power Delivery

voltage corresponds to virtual machine's inner voltage e. From (1)-(10), the control diagram of improved synchronverter is designed as Fig. 4 shows. The whole control diagram consists of an active power-frequency control loop and a reactive power-voltage control loop. Reset 1-Reset 4 are reset switches, which can help reduce the surge currents when switching on the grid-connected circuit breaker.

1) Active power-frequency control loop

In accordance with switch S1's status, there are two control modes for this loop:

a) When S1 is off: It is a traditional synchronverter, grid frequency's changes can be reflected by virtual rotor's speed. When rotor speed ω is too fast or too slow, the input torque will adaptively decrease or increase to regulate the grid frequency. But when the synchronverter enters into a steady state, there exists a frequency error Δf:

$$\Delta f \approx \frac{P^* - P_e}{2\pi D_f \omega^*} \tag{11}$$

Where P_e is the electromagnetic power, P^* is the active power reference value. So even if the VSC converter has sufficient frequency control reserve, the grid frequency will still have a steady state error as calculated by (11). In other words, the synchronverter in [11] has only primary frequency control ability, and cannot achieve secondary regulation.

b) When S1 is on: As Fig. 4 shows, an additional feedback loop is added now, so we get an improved synchronverter. If any difference between ω and ω^* exists, the synchronverter will actively change its active power reference value to $P_m{}'$. Thus if there is enough frequency control reserve at the dc side, and capacity of the VSC converter is large enough, the steady state error of frequency regulation will be eliminated ultimately. I.e., secondary frequency regulation can be realized by the improved synchronverter.

2) Reactive power-voltage control loop

According to the switch status of S1 and S2, there are three control modes for this loop:

a) When S2 is on and S3 is off: *Constant reactive power control mode*, only the converter's reactive power output will be controlled with no error.

b) When S2 is off and S3 is on: *Constant ac voltage control mode*, only the voltage at PCC will be controlled with no error.

c) When both S2 and S3 is on: The reactive power and voltage at PCC will be controlled at the same time, and their control errors obey:

$$\Delta Q + D_u \Delta U = 0 \tag{12}$$

By choosing different values for D_u, different relative control precisions of reactive power output and ac voltage at PCC can be gained. Particularly, when D_u is large enough, this control mode is equal to *Constant ac voltage control mode*, whereas when D_u is very small, it is equivalent to *Constant reactive power control mode*.

3) Switchable current limiting loop

Synchronverter has a defect that when operating as an inverter, it cannot limit its current during abnormal conditions. So a fault may damage its power electronic components or trip it out. Inspired by [10] [24] [25], this article adds a current limiting loop as Fig. 5 shows. ω^* is the reference value of synchronverter's rotor speed, θ is its rotor angle, I_{rated} is its rated phase current magnitude, and m is a multiple designated by us. The m is taken as 1 in this paper.

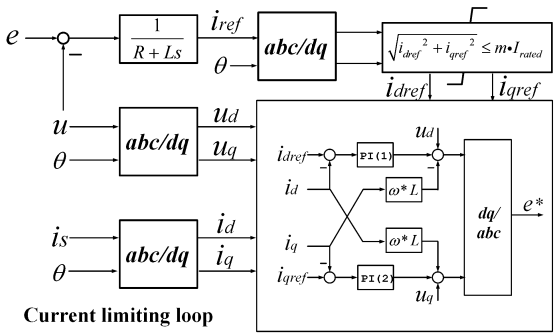

Fig. 5 Current limiting loop of the improved synchronverter

The control principle of this current limiting loop is that: When overcurrent situation occurs, this loop will be switched on quickly, a fast inner current control loop will turn to control synchronverter's inner voltage, and then overcurrent situations can be avoided by limiting the d-q axis current references i_{dref} and i_{qref}. When the current magnitude returns to normal for a certain time interval, e.g., 0.5s, this loop will be switched off. Then the synchronverter's original inner voltage e will be used to generate trigger pulse. Note that e and u are used to generate the current reference value i_{ref}, which can make this current limiting loop switched on seamlessly.

Note that this loop does not need PLL, which is slightly different from the protection loop in [10]. Simulation shows that this current limiting loop is feasible in many cases, but further detailed discussion is needed on whether other methods, e.g., generating a reference phase angle through an integrator, will provide better performance, especially under severe fault conditions. Because in that case, synchronverter's rotor speed may increase or decrease dramatically.

In sum, it can be known from this section that: (i) By changing the switch status of S1, S2 and S3, the improved synchronverter can shift between different control modes; (ii) By a switchable current limiting loop, synchronverter can limit its current during abnormal conditions. Compared to traditional methods, like voltage-oriented vector control or VF-DPC, the improved synchronverter features that: (i) It can offer power supply for weak grids, even passive networks. So it has the black startup ability. (ii) During normal operation and even under fault conditions, it does not need PLL. (iii) It can self-synchronize with the connected ac grid and achieve secondary frequency control.

IV. Control Of The Hybrid MTDC System

In this section, the article will propose and present in detail a novel control strategy for the hybrid MTDC system in Part II. This control is named *active voltage feedback control.*

A qualified control strategy for MTDC system should consider the dc grid's energy balance as well as the connected ac grid's energy balance. I.e., both dc bus voltage and ac grid's

This article has been accepted for publication in a future issue of this journal, but has not been fully edited. Content may change prior to final publication. Citation information: DOI 10.1109/TPWRD.2015.2420657, IEEE Transactions on Power Delivery

frequency should stabilize at its rated value [3][26]. Besides achieving energy balance, *active voltage feedback control* proposed by this paper features that: When integrating volatile and intermittent renewable energies, or experiencing various disturbances, the hybrid MTDC system can run normally without high speed communication system.

In the following part, the *active voltage feedback control* will be introduced in details. First, local control strategies of three VSC stations in the offshore grid are introduced. Then, back on land, local controls of GSINV and GSREC are elaborately explained. After that, we can have a complete picture of the *active voltage feedback control*. Broadly speaking, in the dc grid, the offshore grid part is seen as a current source, GSREC plays the role of a slack bus, and dc voltage is maintained through the cooperation between GSREC and GSINV with no reliance on high speed communication system.

A. Controls of the offshore grid part

TABLE I
CONTROLS OF THE OFFSHORE GRID PART

Island1	Plant1	With governor, excitation device, and PSS installed.
	Plant2	With excitation device and PSS installed. The power input is constant and no governor is equipped here.
	VSC1	Improved synchronverter with S2 off and S3 on.
Offshore Wind farm	PMSG	Maximum power point tracking (MPPT) control
	VSC2	Constant voltage constant frequency control is used so as to inject the maximum power captured by the wind turbine into the dc grid.
Island2	PV Station	Can be connected or disconnected to the grid, if connected, Incremental Conductance Tracking Algorithm is used to track the maximum power point.
	VSC3	Improved synchronverter with S2 off and S3 on.

Controls of different electric components in the offshore grid are indicated in Table I. All excitation devices aim to maintain a constant terminal voltage. To verify the frequency regulation ability of the improved synchronverter, Plant2 has no governor. The offshore wind farm is modelled as a lumped PMSG wind turbine, without considering any interaction between different wind turbines. In total, the offshore grid part can be regarded as a load node in the dc grid. Regardless of line losses, per unit value of the active power which flows from onshore grid to offshore grid is represented as P_{vsc}, $P_{vsc} \in [-0.43, 0.45]$.

B. Controls of GSINV and GSREC

In brief, the control target of GSINV and GSREC is that GSINV can extract a specified amount of dc current from the hybrid MTDC system, GSREC can serve as a slack bus in the dc grid, and dc voltage can be maintained at a desirable value.

1) Local control in GSINV

The dc terminal voltage of GSINV is:

$$U_{dinv} = 2\left(\frac{3\sqrt{2}E}{\pi k_T}\cos\beta_{inv} + \frac{3\omega L_r}{\pi} I_{dinv}\right) \tag{13}$$

Where E is transmission line side voltage of the converter transformer, k_T is the transformer ratio, β_{inv} is the ignition advance angle at the inverter side, L_r is the commutation inductance, and I_{dinv} is the dc current flowing into GSINV.

Fig. 6 shows the control diagram of GSINV and GSREC. In Fig. 6(a), GSINV's local control is displayed. U_{dinv}, I_{dinv} and Overhead Line 2's resistance R_2 are used to calculate the dc voltage at point A, the calculated result is denoted as U_{dmp_inv}. U_{dref}, reference value of dc voltage at point A, is determined by (14). The difference value between U_{dmp_inv} and U_{dref} passes the PI controller PI(1) and gets β_{inv1}, whose control target is to make $U_{dmp\_inv} = U_{dref}$.

$$F_1 : U_{dref} = k_c(I_{dinv} - I_{dinvref}) + 1 \tag{14}$$

Note that $U_{dref} = F_1(I_{dinv})$ is a monotonic increasing function, and $I_{dinvref}$ is the reference value of I_{dinv}. We want GSINV to extract 1000MW active power from dc grid, so here $I_{dinvref}$ is set to 1, i.e., (1, 1) is one point in (14). The

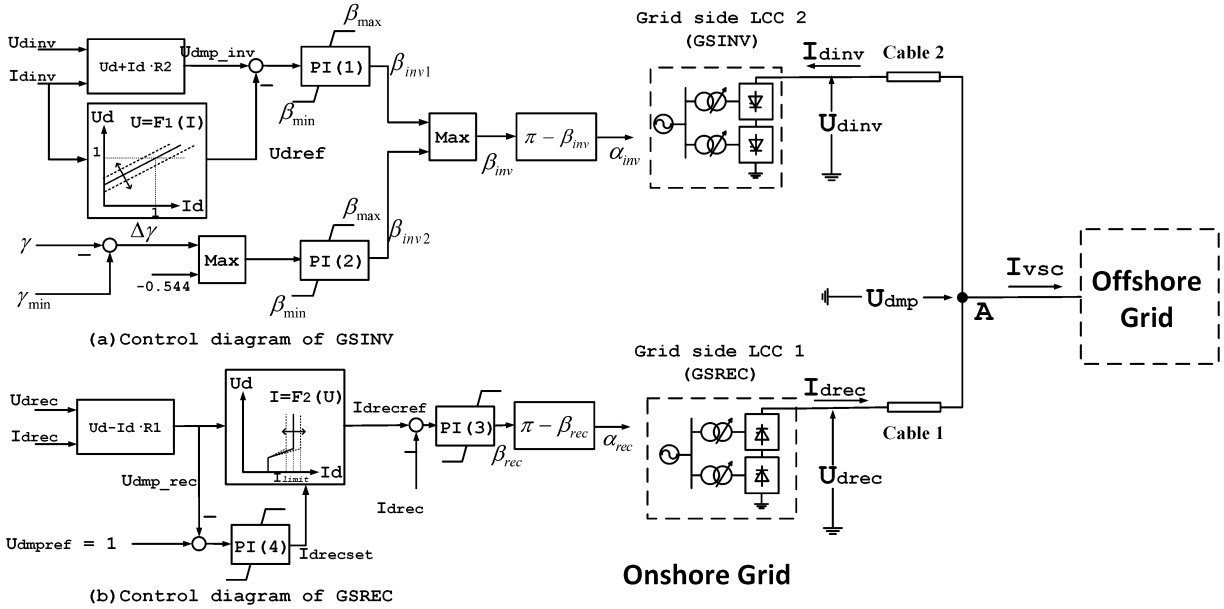

Fig. 6 Control diagrams of GSINV and GSREC

This article has been accepted for publication in a future issue of this journal, but has not been fully edited. Content may change prior to final publication. Citation information: DOI 10.1109/TPWRD.2015.2420657, IEEE Transactions on Power Delivery

parameter k_c needs to be weighed carefully, because it is closely correlated to I_{dinv}'s steady state error, safety margin of the rated operating point, etc. It will be discussed in more details in part *3)*.

From the extinction angle γ and its lower limit value γ_{min}, we can obtain β_{inv2}, which aims to indicate a ceiling voltage to the dc grid, and prevent the commutation failure. After obtaining β_{inv1} and β_{inv2}, we take the maximum and make it β_{inv}, then convert it to the firing angle α_{inv} of GSINV.

In sum, during normal operation, GSINV will determine a reference value of the dc voltage at point A based on I_{dinv}, and then achieve it. According to (14), the larger I_{dinv} is, the bigger U_{dref} will be, and vice versa. That is why this control is called *active voltage feedback control*.

2) Local control in GSREC

The dc side voltage of GSREC is:

$$U_{drec} = 2\left(\frac{3\sqrt{2}E}{\pi k_T}\cos\alpha_{rec} - \frac{3\omega L_r}{\pi} I_{drec}\right) \qquad (15)$$

Where I_{drec} is the dc current flowing out of GSREC, α_{rec} is the firing angle at rectifier side.

GSREC's local control is shown in Fig. 6(b), it includes an outer loop control and an inner loop control. U_{drec}, I_{drec} and Overhead Line 1's resistance R_1 are used to calculate the dc voltage at point A, the result donated as U_{dmp_rec}. But notice that there might be a slight difference between U_{dmp_rec} and U_{dmp_inv} because of line parameter perturbations, voltage harmonics, etc. Then based on (16), I_{drec}'s reference value will be obtained. Note that when dc fault occurs, and dc voltage drops below 0.3 $p.u.$, GSREC will limit its dc current output.

$$F_2: I_{drecref} = \begin{cases} 0.45 & 0 \le U_{dmp\_rec} < 0.2 \\ (10I_{drecset} - 4.5)U_{dmp\_rec} - 2I_{drecset} + 1.35 & 0.2 \le U_{dmp\_rec} < 0.3 \\ I_{drecset} & U_{dmp\_rec} \ge 0.3 \end{cases} \qquad (16)$$

The inner control aims to make GSREC follow outer loop's instruction, then injects a corresponding amount of current into the dc grid. It also contains a constant α control which can ensure the reliable operation of thyristors.

In short, GSREC will adaptively change its output current I_{drec} according to the calculated real time dc voltage U_{dmp_rec}. The higher U_{dmp_rec} is, the more current will be injected by GSREC into the grid, and vice versa.

3) Core control part's interpretation

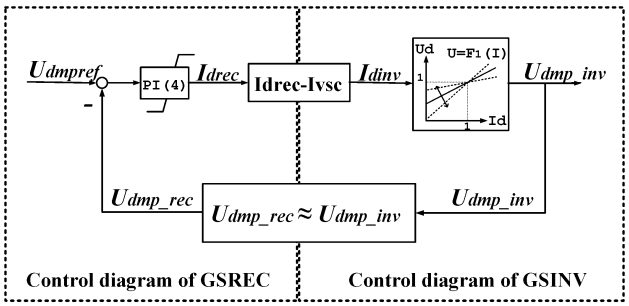

Fig. 7 Core control part of *active voltage feedback control*

If all minor parts are neglected, core control logic of the *active voltage feedback control* can be seen in Fig. 7. The feedback control of dc voltage is completed by GSINV and GSREC's coordination. The whole control strategy does not need high speed communication systems because dc voltage at the point A can serve as an alternative communication signal. E.g., if $I_{dinv} < 1p.u.$, GSINV will actively reduce the dc voltage. After sensing this change, GSREC will increase its current output so that more current will flow into GSINV, and I_{dinv} will stabilize at $1p.u.$ finally.

Fig. 8 shows the current voltage characteristic curves of GSINV, GSREC and the offshore grid. GSREC acts as a slack bus and its operating point can move left or right. But note that we only consider the situation when $U_{dmpref} = 1\ p.u.$ in this paper, if U_{dmpref} can change according to I_{drec} and U_{drec}, the imbalanced power flow from offshore grid might be shared between GSREC and GSINV.

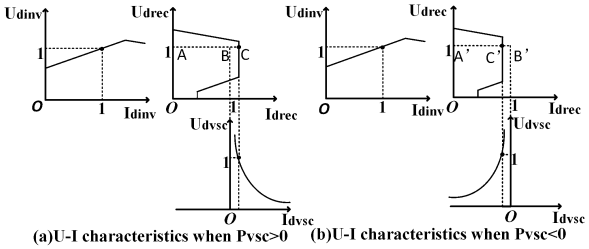

Fig. 8 Current voltage characteristics of the hybrid MTDC system

As mentioned previously, choosing a proper k_c in (14) is very important. If k_c is too small, there will be a steady state error between I_{dinv} and $I_{dinvref}$, which obeys:

$$k_c \approx \frac{\left|U_{dmp\_inv} - U_{dmp\_rec}\right|}{\left|I_{dinv} - I_{dinvref}\right|} \qquad (17)$$

For instance, if k_c is chosen as 0.02, the difference between U_{dmp_rec} and U_{dmp_inv} is 0.001, then the steady state error between I_{dinv} and $I_{dinvref}$ will be 0.05, which is too large. But if k_c is too large, there might be more than one intersection point in GSINV and GSREC's current voltage characteristic curves, which might make our system instable. Given all these, the value of k_c was manually chosen as 0.5 here. But it might not be the optimal one, further study is required.

C. Implementation details

When the whole system starts up, these steps can be followed: (i) the point-to-point HVDC system including GSINV and GSREC starts up with the aid of telecommunication system, then the system switches to *active voltage feedback control*; (ii) in Island 1, VSC1 is unblocked and connected to the dc grid, but its active power output is set to 0; (iii) Plant1 reduces its active power output to 0 slowly, meanwhile VSC1 gradually injects more active power into the AC Grid 1; (iv) VSC2 is unblocked and connected to the dc grid, then the wind turbines at sea are synchronized to the grid group after group to minimize the impact; (v) after the offshore wind farm has been connected to the dc grid, VSC3 is unblocked to power the Island 2; (vi) the PV station can be connected to the AC Grid 2.

This article has been accepted for publication in a future issue of this journal, but has not been fully edited. Content may change prior to final publication. Citation information: DOI 10.1109/TPWRD.2015.2420657, IEEE Transactions on Power Delivery

V. Simulation Results And Analysis

The hybrid MTDC system and its control was modelled in PSCAD/EMTDC, more detailed network parameters can be found in the appendix part. In this part, firstly, frequency regulation abilities of the traditional synchronverter and the improved one were compared to show that the latter could achieve secondary frequency control, and regulate the grid frequency without error. Then the whole hybrid MTDC system was tested under various disturbances, e.g., wind speed variations, solar radiation changes, load fluctuations and even faults, to verify the *active voltage feedback control*'s feasibility. Specially, the improved synchronverter's current limiting ability was verified when an ac fault occurs in Island 1. The hybrid MTDC system can operate normally without high speed communication system during the whole process.

A. Comparison of synchronverter's frequency regulation abilities before and after improvement

TABLE II
Main Simulation Parameters Of Grid In Island 1

	Parameter	Value
VSC1	D_f	304000.0
	J	607.9
	K	93320.0
	D_u	14850.0
	K_p	636.6
	ω^*	100π (rad/s)
	P^*	165 (MW)
Plant2	Inertia constant of SG	4.7 (s)
	Total active power input	82 (MW)

To compare the frequency regulation abilities of traditional synchronverter and the improved one, only the grid on island 1 was used here, and a 500kV dc voltage source was connected to VSC1's dc terminal. Main parameters are given in Table II. When simulation began, all loads at Island 1 were powered by VSC1 and Plant2, the system was stable. Load 4, which is 40MW, was shedded at $t = 1s$ and reconnected to the AC Grid 1 at $t = 10s$. The simulation results were given in Fig. 9. To exaggerate the results, active power input of the prime mover in Plant 2 remained unchanged during the whole process, so it did not help regulate the grid frequency. At $t = 1s$, when 40MW load was shedded, synchronous generators in Plant2 began to accelerate, so did the grid frequency. Once sensing this, whether S1 was switched on or off, synchronverter would reduce its active power output to help restore the grid frequency. During the transient process, maximum frequency deviations of both kinds of synchronverters were less than 0.2Hz.

But during $t \in [5s, 10s]$, if the traditional synchronverter was used, i.e., S1 was switched off, there existed a steady state error as calculated by (11), which was about 0.07Hz. From (11), we could find that besides closely linked with D_f, the frequency regulation error was also proportional to the difference between VSC1's active power reference P^* and its actual active power output. If the improved synchronverter was applied, i.e., S1 was switched on, we could see from Fig. 9(c) that secondary frequency control can be achieved, and grid frequency could

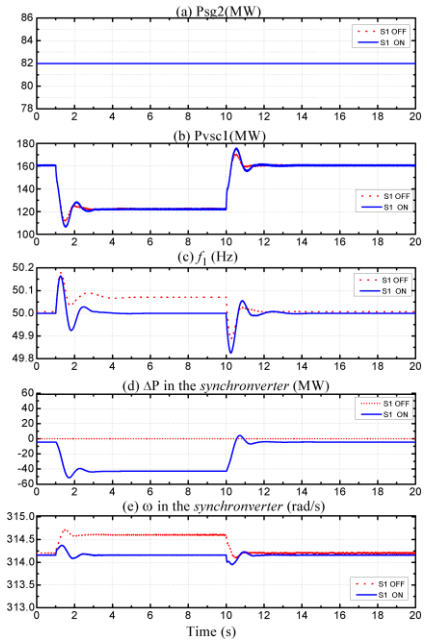

Fig. 9 Comparison of two synchroverters' frequency regulation abilities. (a) Active power input of SGs in Plant2. (b) Active power output of VSC1. (c) Frequency of AC Grid 1. (d) ΔP in the synchronverter. (e) ω in the synchronverter.

always stabilize at 50Hz with no error after each transient process. This was thanks to the added loop which generated ΔP, as shown in Fig. 9(d). From Fig.9(c) and Fig. 9(e), it is obvious that the improved synchronverter synchronized with the grid very well.

A. Verification of active voltage feedback control under normal disturbances

TABLE III
Disturbances That Hybrid MTDC System Subjects To

	Time	Disturbances
Offshore wind farm	t=1s	Wind speed changes from 13m/s to 11m/s.
	t=4s	Wind speed increases from 11m/s to 12m/s.
	t=7s	Wind speed increases from 12m/s to 13m/s.
Island2	t=10s	Solar radiation intensity increases from 600W/m^2 to 1000 W/m^2.
	t=12s	Solar radiation intensity decreases from 1000W/m^2 to 600 W/m^2.
Island1	t=14s	Load 4 is shedded from AC Grid 1.
	t=20s	Load 4 is reconnected to AC Grid 1.

When simulation started, the hybrid MTDC system was in a steady state. All the disturbances during the simulation process were given in Table III, simulation results were shown in Fig. 10.

From Fig. 10 we could see that when wind speed or solar radiation varied, I_{dinv} tended to deviate from its reference value 1 *p.u.*, then this message would be "written" into the dc voltage by GSINV. Once GSREC perceived dc voltage's variation, its firing angle would be adjusted accordingly to change its dc current output. Finally, GSINV's dc current I_{dinv} would stabilize at 1 *p.u.*. When load of the AC Grid 1 fluctuated at $t = 14s$ or $t = 20s$, VSC1 would adaptively change its

This article has been accepted for publication in a future issue of this journal, but has not been fully edited. Content may change prior to final publication. Citation information: DOI 10.1109/TPWRD.2015.2420657, IEEE Transactions on Power Delivery

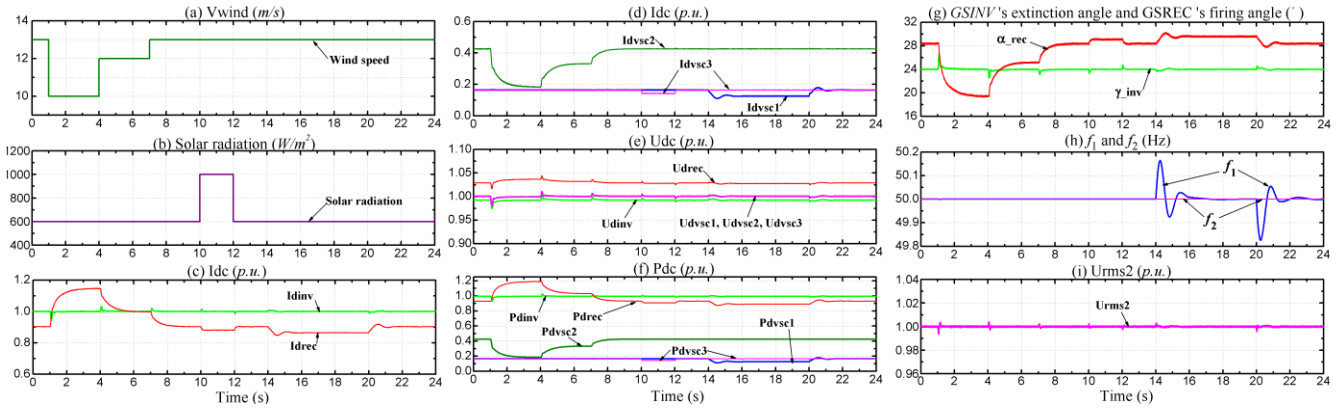

Fig. 10 Simulation results under different kinds of disturbances. (a) Wind speed on the offshore wind farm. (b) Solar radiation intensity in Island 2. (c) DC currents of GSINV and GSREC. (d) DC currents of VSC1, VSC2 and VSC3. (e) DC voltage. (f) DC power. (g) GSINV's extinction angle and GSREC's firing angle. (h) Grid frequencies in Island 1 and Island 2. (i) AC voltage in Island 2.

active power output to regulate the grid frequency. In view of the whole hybrid MTDC system, the load fluctuation in AC Grid 1 would ultimately be balanced by GSREC's output power. During the whole process, there were only some small ripples in GSINV's dc current I_{dinv} and system's dc voltage. Power quality of AC Grid 2 could also be ensured. Note that at about $t = 1.1s$ and $t = 6s$, without reconnecting the dc terminals, power reversal occurred between the onshore part, which consisted of two LCC stations, and the offshore part, which included three VSC stations. This was not possible in two terminal hybrid HVDC systems [1].

B. Fault at the ac side of VSC1

As shown in Fig. 11(a)-(d), a single phase earth fault was applied on Line 3 of the AC Grid 1 at $t = 0.5s$ and with a duration of 100ms. If the current limiting loop does not exist: As the dc capacitor of VSC1 could sustain its output dc voltage when the fault began, this disturbance had little effect on the

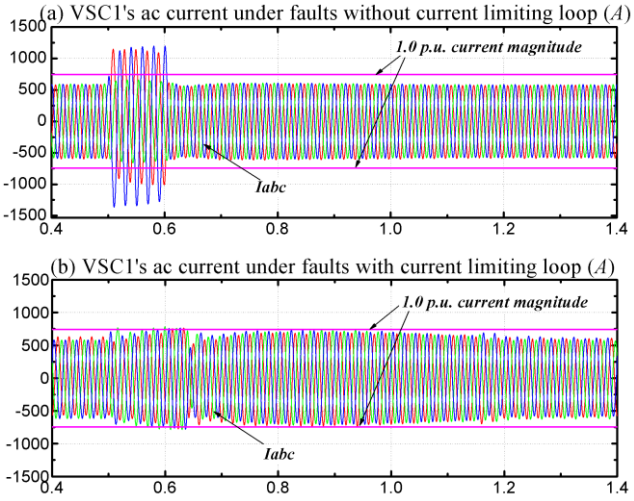

Fig. 12 VSC1's current output under faults

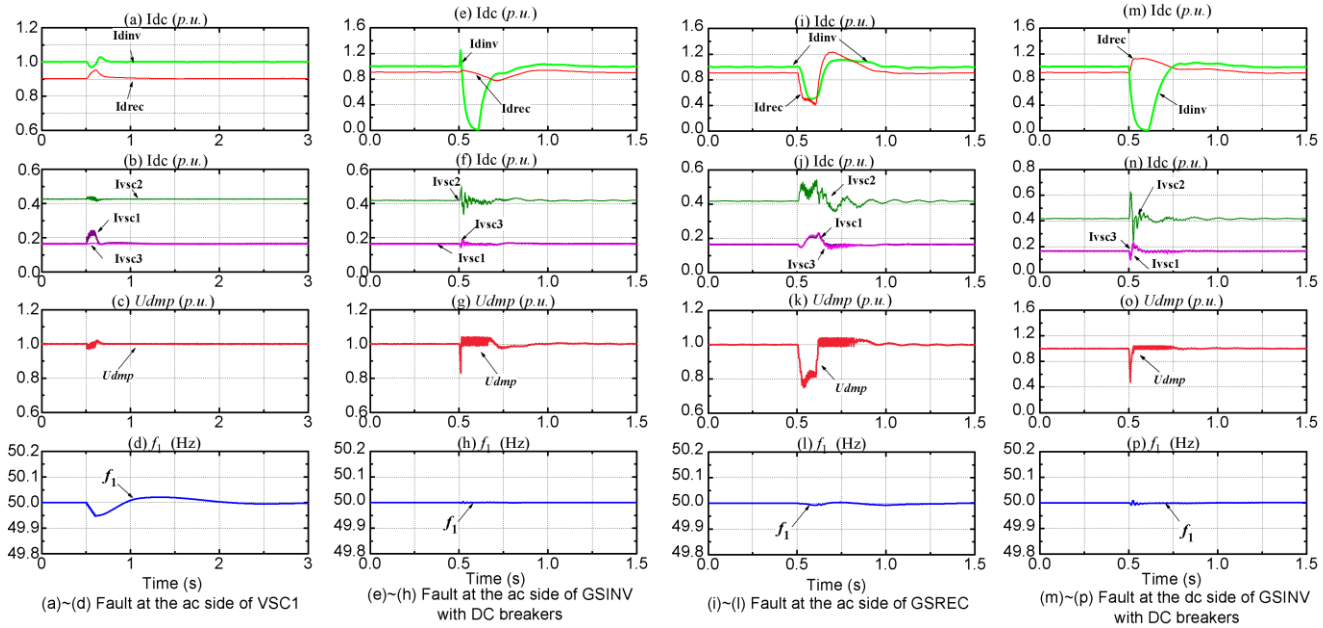

Fig. 11 Simulation results under different kinds of faults. (a)(e)(i)(m) DC currents of GSINV and GSREC. (b)(f)(j)(n) DC currents of VSC1, VSC2 and VSC3. (c)(g)(k)(o) DC voltage at point A in Fig. 1. (d)(h)(l)(p) Grid frequency in Island 1.

This article has been accepted for publication in a future issue of this journal, but has not been fully edited. Content may change prior to final publication. Citation information: DOI 10.1109/TPWRD.2015.2420657, IEEE Transactions on Power Delivery

whole dc system. Dc voltage and all stations' dc currents did not fluctuate much, the system could recover soon. Thanks to synchronverter's control, the frequency of AC Grid 1 stabilized at the rated frequency 50Hz within 2.5s. But as Fig. 12(a) shows, VSC1's current was too large under fault conditions, and this probably damaged the converter. But in this case, *active voltage feedback control*'s feasibility could be better verified by a larger disturbance in dc grid. If the current limiting loop was added, VSC1's current would always be limited in a safe range, as showed in Fig. 12(b). But simulation shows that it will take synchronverter 4.5s to restore the frequency in Island1, which is larger than 2.5s. So it is a trade-off between to limit synchronverter's current and to restore the frequency faster.

C. Fault at the ac side of GSINV

Note that a dc breaker should be installed on Line 2. The simulation results were shown in Fig. 11(e)-(h). At $t = 0.5s$, a single phase earth fault was applied at ac side of the GSINV, and lasted for 100ms. Then the dc voltage decreased rapidly, and I_{dinv} climbed up quickly. The dc breaker operated at $t = 0.51s$ and reclosed 100ms later. To prevent the subsequent overvoltage caused by energy imbalance, a dc damping resistor as described in [32] was installed at point A in Fig. 1, its resistance value was taken as 100Ω. During $t \in [0.51s, 0.61s]$, the dc damping resistor at point A played a role, so the dc voltage oscillated around 1p.u.. Meanwhile, the dc current flowing into GSINV decreased rapidly, because it had been dissociated from the dc system. Currents of GSREC, VSC1, VSC2 and VSC3 showed comparatively little fluctuations. The grid frequency in AC Grid 1 felt little impact from the disturbance. After the dc breaker reclosed again, the whole system restored to its previous steady state within about 0.7s.

D. Fault at the ac side of GSREC

Fig. 11(i)-(l) showed the simulation results. At $t = 0.5s$, a single phase short circuit with a duration of 100ms was introduced at GSREC's ac side. So during $t \in [0.51s, 0.61s]$, there was a 0.2p.u. voltage sag in the dc system. Less current was sent out by GSREC, and the current absorbed by GSINV also decreased by 0.5p.u. The VSC1's output current increased by 0.1p.u., so more current found their paths into VSC1 and VSC2. Meanwhile, there were only small fluctuations in the grid frequency of AC Grid 1.

After the fault disappeared, I_{drec} climbed up quickly, so did the dc voltage. The dc damping resistor at point A saved the dc system from overvoltage again. At last, the whole hybrid MTDC system restored to a steady state within about 1s.

E. DC Line Fault

Cable 3, Cable 4 and Cable 5 are both cross-linked polythene cables, which is characteristic of low fault rate. So here, we supposed that a dc line short circuit fault occurred at the middle of Overhead Line 2. In this case, a dc breaker on Overhead Line 2 was indispensable, otherwise the VSC converters would suffer from serious overcurrent. The dc breaker should be installed close to the point A. The fault began at $t = 0.5s$ and lasted for 100ms, the dc breaker operated at $t = 0.51s$ and reclosed 100ms later.

As Fig. 11(m)-(p) showed, at the beginning of the fault, dc voltage at point A dropped rapidly, the current extracted by GSINV decreased quickly, and GSREC tended to inject more current into the dc grid. The dc capacitor of VSC1, VSC2 and VSC3 discharged, so VSC2's current output showed a rapid increase, meanwhile VSC1 and VSC3 absorbed less current than before. After the dc breaker opened at $t = 0.51s$, GSINV would absorb cleanly all the remaining energy on Overhead Line 2. The GSREC's current output climbed up by about 0.2p.u.. When the system's dc voltage recovered quickly after dc breaker's operation, the "inner voltage" of VSC1 and VSC3 also increased rapidly, so there were slight overshoots in their currents shortly after $t = 0.51s$.

After the fault disappeared, the whole system successfully returned to its previous steady state within 0.7s. During the whole process, the grid frequency in Island 1 remained nearly unchanged. Note that if the dc short circuit fault was permanent, dc breakers should open again. Then the remaining LCC station should switch to constant voltage control.

VI. Conclusion

This article has proposed an idea to integrate more renewable energy, provide remote islands with reliable power supply and regulate their grid frequencies at the same time. The idea is to expand the "West Power to East" point-to-point LCC HVDC link into a hybrid MTDC system. The article has also given detailed implementation methods: (i) improves the traditional synchronverter to achieve secondary frequency control, and be able to limit its current independent of PLL under fault conditions; (ii) proposes a brand new steady state control strategy *active voltage feedback control* for the hybrid MTDC system. The proposed *active voltage feedback control*: (i) makes the system integrate more renewable energy, and offer reliable power supply for remote islands. (ii) During normal operation, it can make the hybrid MTDC system work at a desirable operating point independent of telecommunication system. (iii) With dc breakers and dc damping resistor, the hybrid MTDC system can ride through various faults.

Acknowledgment

The authors would like to thank Prof. Boon Tek Ooi and Prof. Qing-Chang Zhong for their valuable experience and earnest instruct, thank Jan Ackermann, Dr. Jing Wu, Wei Dai for helping us polish up the writing. The authors also want to offer sincere thanks to the Reviewers and the Editors for their valuable and constructive suggestions.

Appendix

AC Grid 1					
	1	2	3	4	5
Load(MVA)	70+j20	100+j35	30+j9	39+j12	
Line impedance(Ω)	4.50+j38.1	6.30+j53.32	4.5+j38.09	14.28+j93.62	2.29+j9.99
AC Grid 2					
	1	2	3	4	5
Load(MVA)	40+j13	55+j18	40+j13	55+j18	
Line impedance(Ω)	6.30+j53.32	4.50+j38.09	6.30+j53.32	5.29+j44.97	
DC Grid					
	1	2	3	4	5
Line resistance(Ω)	8	2	0.83	0.25	0.25
Line reactance(L)	1.9	0.5	0.028	0.008	0.008

This article has been accepted for publication in a future issue of this journal, but has not been fully edited. Content may change prior to final publication. Citation information: DOI 10.1109/TPWRD.2015.2420657, IEEE Transactions on Power Delivery

PI Parameters in Fig. 5				
	PI(1)	PI(2)	PI(3)	PI(4)
k_p	0.7506	0.7506	1.0989	1.0000
k_i	0.0544	0.0544	0.0109	0.0120

Exciter used in Plant 1 and Plant 2 (AC3A)

$T_C = 0,\ T_B = 0,\ T_A = 0.04,\ T_E = 1.17,\ T_F = 0.7,\ u_{AMAX} = 5.49,\ u_{AMIN} = -0.95,$
$u_{EMAX} = u_{E1} = 6.24,\ S_E[u_{E1}] = 1.143,\ u_{E2} = 4.68,\ S_E[u_{E2}] = 0.10,\ E_{fdN} = 2.36,\ K_A = 45.62,$
$K_R = 3.77,\ K_C = 0.104,\ K_D = 0.499,\ K_E = 1.0,\ K_F = 0.05,\ K_N = 0.05, U_{FEMAX} = 16.$

PSS used in Plant 1 and Plant 2 (PSS1A)

$A_1 = 0,\ A_2 = 0,\ T_1 = 1.3,\ T_2 = 0.2,\ T_3 = 1.3,\ T_4 = 0.02,$
$T_5 = 30,\ T_6 = 0,\ K_S = 0.1,\ u_{SMAX} = 0.05,\ u_{SMIN} = -0.05.$

REFERENCES

[1] Zhao Z, Iravani M R. Application of GTO voltage source inverter in a hybrid HVDC link[J]. Power Delivery, IEEE Transactions on, 1994, 9(1): 369-377.

[2] Lu W, Ooi B T. Multi-terminal LVDC system for optimal acquisition of power in wind-farm using induction generators[C]//Power Electronics Specialists Conference, 2001. PESC. 2001 IEEE 32nd Annual. IEEE, 2001, 1: 210-215.

[3] Haileselassie T M, Uhlen K. Primary frequency control of remote grids connected by multi-terminal HVDC[C]//Power and Energy Society General Meeting, 2010 IEEE. IEEE, 2010: 1-6.

[4] Guangkai L, Gengyin L, Haifeng L, et al. Research on hybrid HVDC[C]//Power System Technology, 2004. PowerCon 2004. 2004 International Conference on. IEEE, 2004, 2: 1607-1612.

[5] Torres-Olguin R E, Molinas M, Undeland T M. A controller in dq synchronous reference frame for hybrid HVDC transmission system[C]//Power Electronics Conference (IPEC), 2010 International. IEEE, 2010: 376-383.

[6] Kotb O, Sood V K. A hybrid HVDC transmission system supplying a passive load[C]//Electric Power and Energy Conference (EPEC), 2010 IEEE. IEEE, 2010: 1-5.

[7] Flourentzou N, Agelidis V G, Demetriades G D. VSC-based HVDC power transmission systems: an overview[J]. Power Electronics, IEEE Transactions on, 2009, 24(3): 592-602.

[8] Noguchi T, Tomiki H, Kondo S, et al. Direct power control of PWM converter without power-source voltage sensors[J]. Industry Applications, IEEE Transactions on, 1998, 34(3): 473-479.

[9] Durrant M, Werner H, Abbott K. Model of a VSC HVDC terminal attached to a weak AC system[C]//Control Applications, 2003. CCA 2003. Proceedings of 2003 IEEE Conference on. IEEE, 2003, 1: 178-182.

[10] Zhang L, Harnefors L, Nee H P. Power-synchronization control of grid-connected voltage-source converters[J]. Power Systems, IEEE Transactions on, 2010, 25(2): 809-820.

[11] Zhong Q C, Weiss G. Synchronverters: Inverters that mimic synchronous generators[J]. Industrial Electronics, IEEE Transactions on, 2011, 58(4): 1259-1267.

[12] Zhong Q C, Nguyen P L, Ma Z, et al. Self-synchronized synchronverters: Inverters without a dedicated synchronization unit[J]. Power Electronics, IEEE Transactions on, 2014, 29(2): 617-630.

[13] Chen X, Sun H, Wen J, et al. Integrating wind farm to the grid using hybrid multiterminal HVDC technology[J]. Industry Applications, IEEE Transactions on, 2011, 47(2): 965-972.

[14] Nosaka N, Tsubota Y, Matsukawa K, et al. Simulation studies on a control and protection scheme for hybrid multi-terminal HVDC systems[C]//Power Engineering Society 1999 Winter Meeting, IEEE. IEEE, 1999, 2: 1079-1084.

[15] Nakajima T, Irokawa S. A control system for HVDC transmission by voltage sourced converters[C]//Power Engineering Society Summer Meeting, 1999. IEEE. IEEE, 1999, 2: 1113-1119.

[16] Fuan X F, Cheng S. Performance analysis of a hybrid multi-terminal HVDC system[C]//Electrical Machines and Systems, 2005. ICEMS 2005. Proceedings of the Eighth International Conference on. IEEE, 2005, 3: 2169-2174.

[17] Pan W, Chang Y, Chen H. Hybrid multi-terminal HVDC system for large scale wind power[C]//Power Systems Conference and Exposition, 2006. PSCE'06. 2006 IEEE PES. IEEE, 2006: 755-759.

[18] Jaleeli N, VanSlyck L S, Ewart D N, et al. Understanding automatic generation control[J]. Power Systems, IEEE Transactions on, 1992, 7(3): 1106-1122.

[19] Rebours Y G, Kirschen D S, Trotignon M, et al. A survey of frequency and voltage control ancillary services—Part I: Technical features[J]. Power Systems, IEEE Transactions on, 2007, 22(1): 350-357.

[20] Wood A J, Wollenberg B F. Power generation, operation, and control[M]. John Wiley & Sons, 2012.

[21] DeMarco C L, Baone C A, Han Y, et al. Primary and secondary control for high penetration renewables[J]. The Future Grid to Enable Sustainable Energy Syst, 2012.

[22] Krause P C, Wasynczuk O, Sudhoff S D, et al. Analysis of electric machinery and drive systems[M]. John Wiley & Sons, 2013.

[23] Zeng G, Rasmussen T W, Ma L, et al. Design and control of LCL-filter with active damping for Active Power Filter[C]//Industrial Electronics (ISIE), 2010 IEEE International Symposium on. IEEE, 2010: 2557-2562.

[24] Etemadi A H, Iravani R. Overcurrent and overload protection of directly voltage-controlled distributed resources in a Microgrid[J]. Industrial Electronics, IEEE Transactions on, 2013, 60(12): 5629-5638.

[25] Ashabani M, Mohamed Y A R I. Integrating VSCs to weak grids by nonlinear power damping controller with self-synchronization capability[J]. Power Systems, IEEE Transactions on, 2014, 29(2): 805-814.

[26] Barker C D, Whitehouse R. Autonomous converter control in a multi-terminal HVDC system[C]//AC and DC Power Transmission, 2010. ACDC. 9th IET International Conference on. IET, 2010: 1-5.

[27] Beck H P, Hesse R. Virtual synchronous machine[C]//Electrical Power Quality and Utilisation, 2007. EPQU 2007. 9th International Conference on. IEEE, 2007: 1-6.

[28] Driesen J, Visscher K. Virtual synchronous generators[C]//Power and Energy Society General Meeting-Conversion and Delivery of Electrical Energy in the 21st Century, 2008 IEEE. IEEE, 2008: 1-3

[29] Xu L, Williams B W, Yao L. Multi-terminal DC transmission systems for connecting large offshore wind farms[C]//Power and Energy Society General Meeting-Conversion and Delivery of Electrical Energy in the 21st Century, 2008 IEEE. IEEE, 2008: 1-7.

[30] Ma Z, Zhong Q C, Yan J D. Synchronverter-based control strategies for three-phase PWM rectifiers[C]//Industrial Electronics and Applications (ICIEA), 2012 7th IEEE Conference on. IEEE, 2012: 225-230.

[31] Ashabani M, Mohamed Y A R I. Novel comprehensive control framework for incorporating VSCs to smart power grids using bidirectional synchronous-VSC[J]. 2014.

[32] Xu L, Yao L. DC voltage control and power dispatch of a multi-terminal HVDC system for integrating large offshore wind farms[J]. IET renewable power generation, 2011, 5(3): 223-233.

Shuan Dong was born in Shandong, China, in February 1990. He received the B.S. degree from Tianjin University, China in 2012, in Electrical Engineering, and is a postgraduate student in Renewable Energy Department, China Electric Power Research Institute (CEPRI) now. His main field of interest includes HVDC and wind turbine modelling.

Yong-Ning Chi received the B.S. degree in Electric Power Engineering from Shandong Polytechnic University in 1995, the M.S. degree in Electrical Engineering from Shandong University in 2003, and the Ph.D. degree from CEPRI in 2006. He is the Chief Engineer, Renewable Energy Department, CEPRI, and interested in renewable energy integration.

Yan Li received the B.S. degree from Shandong University of Technology in 1999, the M.S. degree from Fuzhou University in 2002, and the Ph.D. degree from China Electric Power Research Institute (CEPRI) in 2007. His interested researches are the renewable energy modeling and grid integration simulation.